Wearable and sensitive heart-rate detectors based on PbS quantum dot and multiwalled carbon nanotube blend film

Liang Gao, Dongdong Dong, Jungang He, Keke Qiao, Furong Cao, Min Li, Huan Liu, Yibing Cheng, Jiang Tang, and Haisheng Song

Citation: Appl. Phys. Lett. **105**, 153702 (2014); doi: 10.1063/1.4898680
View online: https://doi.org/10.1063/1.4898680
View Table of Contents: http://aip.scitation.org/toc/apl/105/15
Published by the American Institute of Physics

Wearable and sensitive heart-rate detectors based on PbS quantum dot and multiwalled carbon nanotube blend film

Liang Gao,[1] Dongdong Dong,[1] Jungang He,[2] Keke Qiao,[1] Furong Cao,[3] Min Li,[2] Huan Liu,[2] Yibing Cheng,[1] Jiang Tang,[1,a)] and Haisheng Song[1,a)]
[1]*Wuhan National Laboratory for Optoelectronics (WNLO), Huazhong University of Science and Technology, 1037 Luoyu Road, Wuhan, Hubei 430074, People's Republic of China*
[2]*School of Optical and Electronic Information, Huazhong University of Science and Technology, 1037 Luoyu Road, Wuhan, Hubei 430074, People's Republic of China*
[3]*Air Force Early Warning Academy, Wuhan, Hubei 430019, People's Republic of China*

(Received 27 July 2014; accepted 7 October 2014; published online 16 October 2014)

Wearable and sensitive photodetectors (PDs) have been demonstrated based on a blend film of PbS quantum dots (QDs) and QDs modified multiwalled carbon nanotubes (MWCNTs). Owing to the synergetic effect from high light sensitivity of PbS QDs and excellent conductive and mechanical properties of MWCNTs, the blend PDs show high sensitivity and flexibility performance: device responsivity and detectivity reach 583 mA/W and 3.25×10^{12} Jones, respectively, and could stand large number (at least 10 000 cycles) and wide angle (up to 80°) bending. Furthermore, the wearable and sensitive PDs have been applied to measure the heart rate in both red and near infrared (NIR) ranges. The presented PDs are expected to work as sensor candidates in integrated electronic skin. © *2014 AIP Publishing LLC*. [http://dx.doi.org/10.1063/1.4898680]

Future electronics are expected to be flexible and comfortable for user-friendly applications.[1–4] As one kind of sensor electronics, electronic skin[1] has received intense research interest due to its comfort and convenience for physiological measurement[1] and wide applications in intelligent robot technology.[2] To match flexibility of electronic skin, active materials of devices have to possess bendable capacity[3,4] in addition to other superior properties. The solution processibility and high near infrared (NIR) sensitivity of PbS quantum dots (QDs)[5] make it possible to be applied as active materials for sensors of electronic skin. However, the mobility of PbS QD film is a little low at 10^{-3}–10^{-4} cm^2/Vs.[6–9] On the other hand, multiwalled carbon nanotubes (MWCNTs) have been shown excellent charge transport (mobility $\sim 10^4$ cm^2/Vs) and mechanical flexibility.[10–12] For PbS QDs and CNTs hybrid system, efficient charge transfer has been observed from photo-excited PbS QDs to CNTs.[13–15] Therefore, the blend of PbS QDs and MWCNTs working as active materials of photodetectors (PDs) makes it possible to implement the synergetic effect of high sensitivity and flexibility, both of which are crucial for electronic skin applications.

In the present contribution, we fabricated three types of conductive PDs based on different blending styles of MWCNTs and PbS QDs. The first type only contained QDs. The second one was named as physically mixing blend (PMB), made up of physically mixed MWCNTs and QDs. And the last one was denoted as chemically anchoring blend (CAB) which consisted of PbS QDs and MWCNTs chemically anchored by QDs. All of the PDs were fabricated on PET (polyethylene terephthalate) substrate. The CAB PDs obtained an estimated detectivity of 3.25×10^{12} Jones, which was 2 times that of PMB PDs and 3.6 times that of PbS QDs alone based ones. And, the CAB PDs could stand large number and wide angle bending, while the pure PbS QDs ones failed. What is more, we further applied the CAB PDs for heart-rate detection as a preliminary demonstration of their potential application for electronic skin.

PbS QDs were synthesized using a modified Hines method.[16] MWCNTs were synthesized by traditional chemical vapor deposition method with the length and diameter ranges of 5–15 μm and 40–80 nm, respectively. The raw-MWCNTs were purified and then dispersed in chloroform. The procedure of PbS QDs anchoring onto MWCNTs is schematically displayed in Fig. 1(a). The grafting was implemented by simply stirring 2 ml of oleic acid (OA)-passivated PbS QDs toluene solution (50 mg/ml) and 1 ml of MWCNTs chloroform solution (1 mg/ml) together at room temperature for 3 days. Figure 1(b) shows the FTIR spectra of PbS QDs, MWCNTs, and MWCNTs grafted by PbS QDs (MWCNT/PbS QD) samples. The MWCNT/PbS QD samples were obtained by centrifuging the above stirred blending solution at 5000 RPM. At such rotation speed, the non-grafted PbS QDs could not be precipitated in centrifuged products. The typical peaks of functional groups such as $(C–H)_{s,as}$ and $(CO_2)_{s,as}$[17] reveal the existence of grafted PbS QDs in the centrifuged products and the chemically anchoring relationship between MWCNTs and PbS QDs. The above grafting result is due to Van der Waals force between OA ligands and MWCNTs, which comes from the interaction of long carbon chains.[14] Single MWCNT grafted by QDs was further characterized by transmission electron microscopy (TEM) and high resolution transmission electron microscopy (HRTEM). Figure 1(c) shows a typical TEM image of MWCNT/PbS QD nanoarchitecture, which clearly reveals the coupling of PbS QDs to MWCNTs. HRTEM image (Fig. 1(d)) confirms the lattice spacing of PbS QD and MWCNT and the chemically anchoring relationship between them.

a)Authors to whom correspondence should be addressed. Electronic addresses: jtang@mail.hust.edu.cn and songhs-wnlo@mail.hust.edu.cn

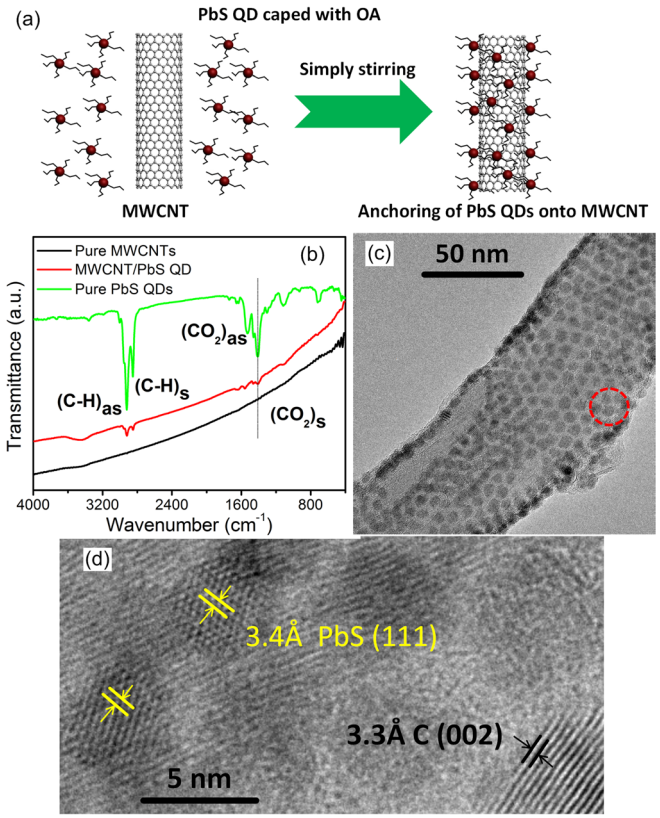

FIG. 1. (a) Schematic description of PbS QDs chemically anchoring onto MWCNTs. (b) FTIR spectra of MWCNTs, PbS QDs, and PbS QD/MWCNT nanoarchitectures. (c) TEM and (d) HRTEM images of PbS QD/MWCNT nanoarchitecture.

Photoluminescence (PL) measurement is traditionally utilized to check the carrier transfer in hybrid system.[13–15] Figure 2(a) shows PL spectra of CAB solution with different MWCNT-to-QD weight ratios. Compared to pure PbS QD, the PL intensities of CABs (1 wt. % and 5 wt. %) decrease dramatically. The schematic image of energy level alignment

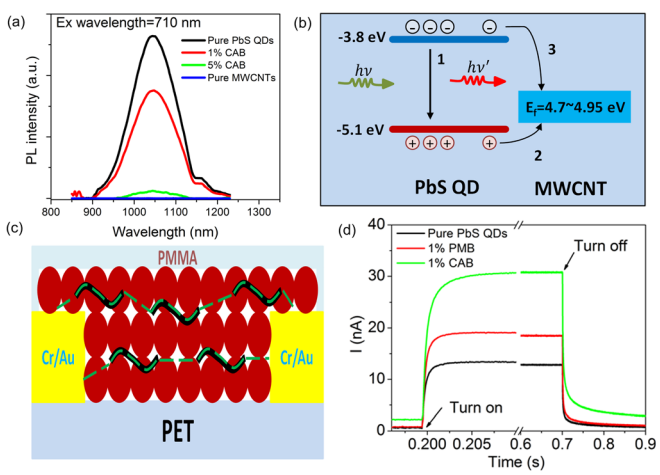

FIG. 2. (a) Steady-state PL spectra of CAB solution with different MWCNT-to-QD weight ratios. (b) Schematic band diagram of MWCNT/PbS QD nanoarchitecture: "1" process represents the recombination of electrons and holes, "2" and "3" processes represent the transfer of holes and electrons from PbS QDs to MWCNTs. (c) Schematic diagram of CAB PD structure, dashed line shows the possible charge transport path (solid black tubes denote MWCNTs and red spheres represent QDs). (d) I-t responses of PbS QDs, PMB, and CAB PDs.

for the hybrid system is shown in Fig. 2(b). For the present system, the conduction band minimum (CBM) and valence band maximum (VBM) of PbS QDs are taken to be −3.8 and −5.1 eV,[18] and the work function of MWCNT is known in the range of 4.7–4.95 eV.[19,20] The relative energy level alignment favors more photo-excited holes than electrons transfer from PbS QDs to MWCNTs.[21] Hence, the photo-induced charges energetically transfer from PbS QDs to MWCNTs ("2" and "3" processes in Fig. 2(b)), which leads to the decrease of PL intensity.

Based on the charge-transfer mechanism, an enhanced conductive PD displayed in Fig. 2(c) was designed and implemented. PET treated by ultraviolet ozone was utilized as the transparent and flexible substrate. Figure 2(c) shows the schematic device structure with the dimension of 15 mm in length and 0.2 mm in width. The metal electrodes (Cr/Au) were pre-deposited by magnetron sputtering in order to obtain both good adhesion on PET and ohmic contact with the active film. The active film was deposited via layer-by-layer spin-coating and later passivated by MPA (3-Mercaptopropionic acid) from a traditional solid state ligand exchanging process.[22] All devices were baked at 90 °C in air for 10 min and finally encapsulated by PMMA (polymethyl methacrylate).

The response current-time (I-t) curves shown in Fig. 2(d) were obtained under 650 nm monochromatic light illumination with an intensity of 430 μW/cm^2. Under an external bias of 5 V, the dark and photocurrent of PDs based on pure PbS QDs, 1 wt. % PMB and 1 wt. % (optimized proportion) CAB are 0.26 nA and 12.9 nA; 0.36 nA and 18.5 nA; and 0.96 nA and 30.3 nA, respectively. The rise time and decay time of CAB PDs are 0.7 ms and 3.8 ms, respectively. And, the PDs are fast enough for 100 Hz signal. Agreeing well with the PL analysis, the incorporation of MWCNT can improve conductivity of the active film. The chemically anchoring contact of PbS QDs with MWCNTs and their energy level alignment favor holes inject into MWCNT, which greatly improves the carrier lifetime and charge transport.

Responsivity (R) and detectivity (D^*) are the two most important figures of merit for PDs. Responsivity measures device sensitivity toward light detection calculated from the following equation:

$$R = (I_{photo} - I_{dark})/P, \tag{1}$$

where I_{photo} is photocurrent, I_{dark} is dark current, and P is the light power impinging onto the device. D^*, normalized detectivity in Jones, is given by the following:

$$D^* = (A\Delta f)^{1/2} R/i_n, \tag{2}$$

where A is the effective area of the detector in cm^2, Δf is the electrical bandwidth in Hz, and R in A/W is measured under the same conditions as the noise current i_n.

There are three contributions to the noise that limit D^*: shot noise from dark current, Johnson noise, and thermal fluctuation noise.[23] Shot noise (I_{sh}), associated with current fluctuation flowing cross a PD, is often dominating the total noise of the detector.[24] Shot noise is determined by dark

current I_{dark} and electrical noise bandwidth Δf through the equation (where q is elementary charge):

$$I_{sh} = \sqrt{2qI_{dark}\Delta f}. \tag{3}$$

Here i_n is equivalent as I_{sh}, we could further simplify the normalized detectivity D^* as

$$D^* = \frac{(I_{photo} - I_{dark})\sqrt{A}}{P\sqrt{2qI_{dark}}}. \tag{4}$$

As shown in Figs. 3(a) and 3(b), the estimated R increases linearly with bias under 650 nm monochromatic illumination at an intensity of $0.2\,\mu\mathrm{W/cm^2}$, while D^* increases nonlinearly. The above results are consistent with the bias depending relationship of Eqs. (1) and (4). Under a bias of 40 V, the obtained R and D^* of 1 wt. % CAB PDs can reach 583 mA/W and 3.25×10^{12} Jones, respectively, which are both about 3.6 times those of pure PbS QDs PDs and 2 times those of 1 wt. % PMB PDs. In Fig. 3(c), the estimated R decreased under a bias of 5 V when the illumination intensity increased, which is due to that deep trap centers contributing significantly to R. Responsivity was filled under high power illumination,[25,26] in addition to more severe bimolecular recombination loss under stronger illumination.

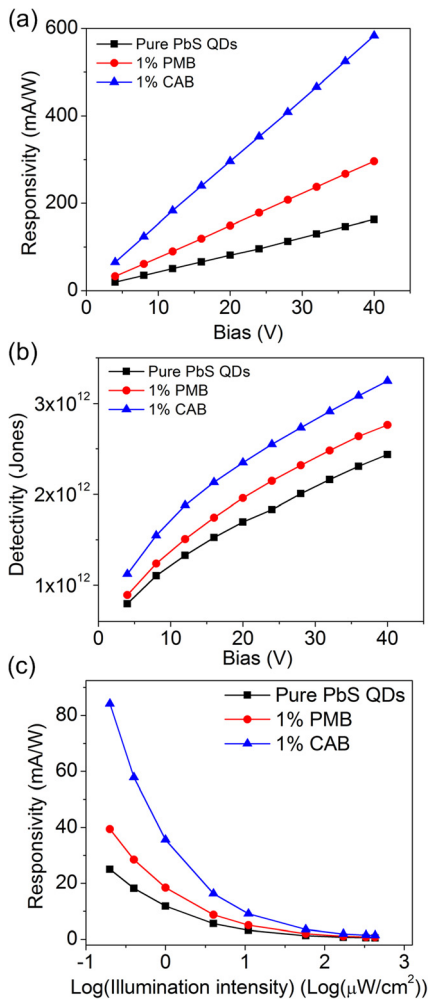

FIG. 3. Detector performance evolution of PbS QDs, PMB, and CAB PDs under different bias voltages ((a) and (b)) and different illumination intensities (c).

Flexibility performances of two-group PDs based on pure PbS QDs (Figs. 4(a) and 4(c)) and 1 wt. % CAB (Figs. 4(b) and 4(d)) was examined at 10 V bias under 650 nm illumination with a power density of $430\,\mu\mathrm{W/cm^2}$. At fixed angle (20°), the I-t evolution curves as the bending cycle are shown in Figs. 4(a) and 4(b). The photocurrents of pure PbS QD PDs shrink ~10% after 10 000 cycles of bending. However, the photocurrents of CAB PDs remain almost the same after the same bending cycles. Figures 4(c) and 4(d) show the flexibility performance of PDs bended at wide angle (10°–80°). Once the PbS QD PDs are bended up to 80°, about 50% attenuation of photocurrent appears. In contrast, the CAB PDs keep almost the same response at above bending angles. Hence, the incorporation of MWCNT can greatly improve the flexibility of PDs in addition to the improvement of film conductivity.

The present superior performance of CAB PDs makes them suitable for skin electronics. The traditional (clipped at middle finger) and CAB (worn at forefinger) based heart-rate detectors are shown in Fig. 5(a). Figure 5(b) demonstrates the measuring state of CAB PDs illuminated by red LEDs. As like the traditional heart-rate signal in Fig. 5(c), the untreated and unfiltered heart-rate signals (Fig. 5(d) and 5(e)) measured in the red and infrared spectral ranges clearly show the relevant features of the pulse, including heart rate, systole, diastole, and the pulse wave reflection. Compared with the traditional heart-rate senor probe, the advantages of the CAB PDs are their smaller size, wider excitation spectra, and friendly and comfortable measurements, which make them capable to work as wearable sensors in wide application fields.

In summary, we have implemented highly flexible and sensitive CAB PDs for heart-rate detection. The chemically anchoring relationship between PbS QDs and MWCNTs and their energy alignment favors the charge transfer from PbS QDs to MWCNTs. Because of the synergetic effect from PbS QDs and MWCNTs, the obtained responsivity and

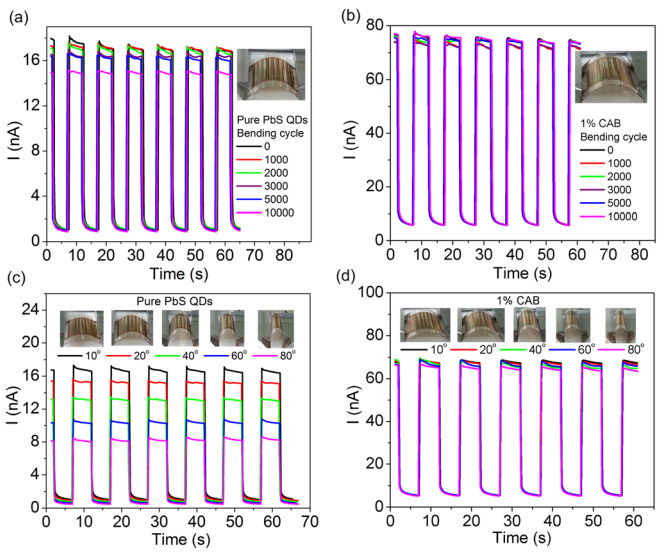

FIG. 4. Flexibility performances of PbS QDs and CAB PDs: (a) and (b) I-t response after different bending cycles at 20°; (c) and (d) I-t response after bending at wide angles (10°–80°). The insets show bending photographs of PDs.

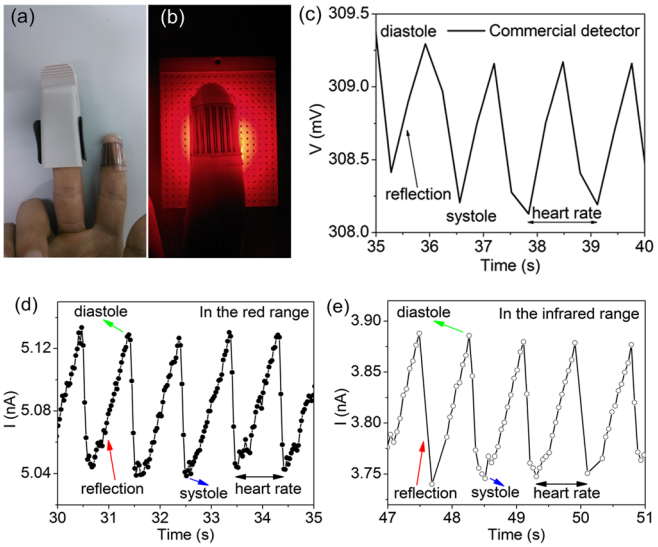

FIG. 5. (a) Comparison between traditional heart-rate sensor probe (clipped at middle finger) and the CAB PDs (worn at forefinger). (b) Heart-rate test of the CAB PDs under red LEDs. (c) The heart-rate signal measured via the traditional detector. (d) and (e) The original heart-rate signal measured through the CAB PDs in the red and infrared spectral ranges.

detectivity of CAB PDs are superior to those of PMB and PbS QD PDs, reaching 583 mA/W and 3.25×10^{12} Jones respectively. For flexibility performance, the CAB PDs can stand large number (at least 10 000 cycles) and wide angle (up to 80°) bending while the pure PbS QDs PDs declines with increasing bending cycles and angles. The CAB PDs have been applied in skin electronics as heart-rate sensors. The output signal can clearly demonstrate the patient heart-rate variation. The synergetic effect and superior device performance are expected to open promising opportunities for functional material selection, device design and implementation of integrated electronic skin.

This work was financially supported by the National Natural Science Foundation of China (61306137, 61274055), by the Independent Innovation Fund of Huazhong University of Science and Technology (HUST: 2013NY002) and by the seed project of Wuhan National Laboratory for Optoelectronics. The authors thank Testing Center of HUST and the Center for Nanoscale Characterization and Devices, Wuhan National Laboratory for Optoelectronics (WNLO) for facility access.

[1]D.-H. Kim, N. Lu, and R. Ma, Science **333**, 838 (2011).
[2]A. N. Sokolov, B. C. Tee, C. J. Bettinger, J. B.-H. Tok, and Z. Bao, Acc. Chem. Res. **45**, 361 (2012).
[3]K. Takei, Z. Yu, M. Zheng, H. Ota, T. Takahashi, and A. Javey, Proc. Natl. Acad. Sci. U.S.A. **111**, 1703 (2014).
[4]J. A. Rogers, T. Someya, and Y. Huang, Science **327**, 1603 (2010).
[5]G. Konstantatos, I. Howard, A. Fischer, S. Hoogland, J. Clifford, E. Klem, L. Levina, and E. H. Sargent, Nature **442**, 180 (2006).
[6]E. J. Klem, H. Shukla, S. Hinds, D. D. MacNeil, L. Levina, and E. H. Sargent, Appl. Phys. Lett. **92**, 212105 (2008).
[7]M. H. Zarghami, Y. Liu, M. Gibbs, E. Gebremichael, C. Webster, and M. Law, ACS Nano **4**, 2475 (2010).
[8]K. S. Jeong, J. Tang, and H. Liu, ACS Nano **6**, 89–99 (2012).
[9]N. Zhao, T. P. Osedach, L.-Y. Chang, S. M. Geyer, D. Wanger, M. T. Binda, A. C. Arango, M. G. Bawendi, and V. Bulovic, ACS Nano **4**, 3743 (2010).
[10]K. S. Novoselov, A. K. Geim, S. Morozov, D. Jiang, Y. Zhang, S. Dubonos, I. Grigorieva, and A. Firsov, Science **306**, 666 (2004).
[11]M.-F. Yu, O. Lourie, M. J. Dyer, K. Moloni, T. F. Kelly, and R. S. Ruoff, Science **287**, 637 (2000).
[12]D. Estrada, S. Dutta, A. Liao, and E. Pop, Nanotechnology **21**, 085702 (2010).
[13]I. Ka, V. Le Borgne, D. Ma, and M. A. El Khakani, Adv. Mater. **24**, 6289 (2012).
[14]D. Wang, J. K. Baral, H. Zhao, B. A. Gonfa, V. V. Truong, M. A. El Khakani, R. Izquierdo, and D. Ma, Adv. Funct. Mater. **21**, 4010 (2011).
[15]D. S. Yu, Y. J. Chen, B. J. Li, X. D. Chen, and M. Q. Zhang, Appl. Phys. Lett. **90**, 161103 (2007).
[16]M. A. Hines and G. D. Scholes, Adv. Mater. **15**, 1844 (2003).
[17]J. Tang, K. W. Kemp, and S. Hoogland, Nat. Mater. **10**, 765 (2011).
[18]J. Tang, L. Brzozowski, and A. R. Barkhouse, ACS Nano **4**, 869 (2010).
[19]M. Shiraishi and M. Ata, Carbon **39**, 1913 (2001).
[20]P. Liu, Q. Sun, F. Zhu, K. Liu, K. Jiang, L. Liu, Q. Li, and S. Fan, Nano Lett. **8**, 647 (2008).
[21]D. Zhang, L. Gan, Y. Cao, Q. Wang, L. Qi, and X. Guo, Adv. Mater. **24**, 2715 (2012).
[22]A. G. Pattantyus-Abraham, I. J. Kramer, and A. R. Barkhouse, ACS Nano **4**, 3374 (2010).
[23]X. Gong, M. Tong, and Y. Xia, Science **325**, 1665 (2009).
[24]E. Heves, C. Ozturk, V. Ozguz, and Y. Gurbuz, IEEE Electron Device Lett. **34**, 662 (2013).
[25]N. C. Greenham, X. Peng, and A. P. Alivisatos, Phys. Rev. B **54**, 17628 (1996).
[26]S. A. McDonald, G. Konstantatos, S. Zhang, P. W. Cyr, E. J. Klem, L. Levina, and E. H. Sargent, Nat. Mater. **4**, 138 (2005).